












A facile approach to fabricate highly sensitive, flexible strain sensor based on elastomeric/graphene platelet composite film

Qingshi Meng^{1,*} , Zhiwen Liu¹ , Sensen Han¹ , Lisheng Xu² , Sherif Araby^{1,3,4} , Rui Cai⁵ , Yu Zhao¹ , Shaowei Lu^{1,*} , and Tianqing Liu⁶ 

¹ College of Aerospace Engineering, Shenyang Aerospace University (SAU), Shenyang 110136, China

² School of Sino-Dutch Biomedical and Information Engineering, Northeastern University, Shenyang 110819, Liaoning, China

³ School of Engineering, University of South Australia, Adelaide, SA 5095, Australia

⁴ Department of Mechanical Engineering, Benha Faculty of Engineering, Benha University, Benha, Egypt

⁵ School of Mechanical, Aerospace and Automotive Engineering, Coventry University, Coventry, UK

⁶ QIMR Berghofer Medical Research Institute, Brisbane, QLD 4006, Australia

Received: 18 February 2019

Accepted: 19 April 2019

Published online:

29 April 2019

© Springer Science+Business Media, LLC, part of Springer Nature 2019

ABSTRACT

This work developed a facile approach to fabricate highly sensitive and flexible polyurethane/graphene platelets composite film for wearable strain sensor. The composite film was fabricated via layer-by-layer laminating method which is simple and cost-effective; it exhibited outstanding electrical conductivity of 1430 ± 50 S/cm and high sensitivity to strain (the gauge factor is up to 150). In the sensor application test, the flexible strain sensor achieves real-time monitoring accurately for five bio-signals such as pulse movement, finger movement, and cheek movement giving a great potential as wearable-sensing device. In addition, the developed strain sensor shows response to pressure and temperature in a certain region. A multifaceted comparison between reported flexible strain sensors and our strain sensor was made highlighting the advantages of the current work in terms of (1) high sensitivity (gauge factor) and flexibility, (2) facile approach of fabrication, and (3) accurate monitoring for body motions.

Introduction

Within the last two decades, strain sensors were widely used in various fields and applications, such as aerospace, automotive, construction, biomedical and other new energy fields [1–5]. Since strain sensor has the ability to detect mechanical deformations due

to external loads, it has attracted considerable interests for various wearable devices to transform human physical motion to electric signals for disease diagnosis, therapy, and health conditions monitoring [6–10]. In most cases, strain sensor is based on piezo-resistance theory in which mechanical deformations translate into resistance changes by strain gauge and

Address correspondence to E-mail: mengqingshi@hotmail.com; lushaowei_2005@163.com

finally monitored by electric signal. At present, the commonly used strain sensors are made of rigid materials such as copper-nickel and nichrome alloy. These types of strain sensors are accurate in measurement, reliable and produced in large scale. However, their main limitations that they are made of rigid materials featuring low gauge factor and hence low sensitivity. Thus, they are not able to detect large deformation on complex curved surface or monitor body motions as a wearable device. The strain sensor based on flexible conductive composites possesses high flexibility and gauge factor, and able to detect small to large strain deformations.

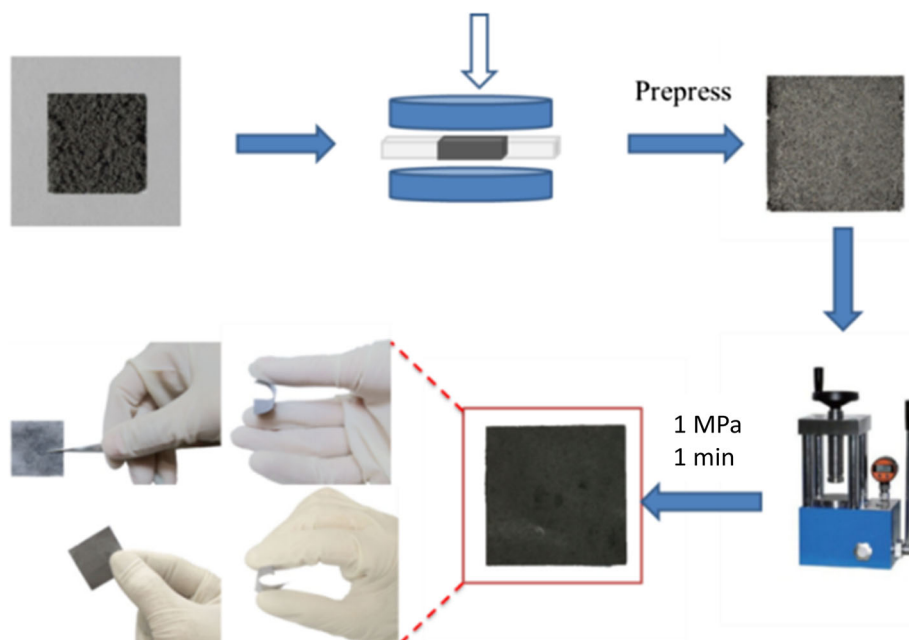
There are various conductive nanomaterials including metals (gold nanoparticle, gold and silver nanowires) and carbon-based nanomaterials such as carbon blacks (CBs) and carbon nanotubes (CNTs), which have been extensively studied in developing flexible strain sensors [11–16]. Although metal-based nanomaterials are stable, most of them are costly and poorly stretchable, and they are susceptible to oxidation when they are used in wearable devices [17, 18]. CBs and CNTs show advantages of lightweight and desirable sensitivity, but they also have limitations; CB-based polymer composites show relatively low electrical conductivity due to its low dimensionality (aspect ratio) which is detrimental to strain sensor, and CB has harmful effect on human health [19–21]. Single-walled carbon nanotubes (SWCNTs) have fascinating properties in strain gauging performances and conductivity, but high cost and difficulty in large-scale industrial production limit their application. Multi-walled carbon nanotubes (MWCNTs) are relatively cheaper with similar properties. However, both of them are not favorable in developing thin-films composite due to their highly entangled structure [17, 22–24]. Therefore, it is a formidable challenge to select novel conductive materials to fabricate highly stretchable and flexible strain sensors.

Graphene has attracted enormous interest in fabrication of flexible strain sensors due to its exceptional properties—Young's modulus 1 TPa, tensile strength 130 GPa, stretch ability up to 25%, and electrical conductivity 6000 S/cm [25, 26]. Pristine graphene and graphene fabricated by CVD are not cost-effective with poor reproducibility and controllability on size dimensions [27]. Graphene oxide and reduced graphene oxide [28] are other derivatives of graphene; their fabrication process needs strong acids

and large quantities of other chemicals. Fabrication process takes dozens of hours, and the yield is not scalable [29]. Additionally, it is limited by low structural integrity implying unsatisfactory electrical conductivity [30]. More recently, graphene platelets (GnPs) have been reported to demonstrate the following advantages: (1) high electrical conductivity of 1460 S/cm, (2) each platelet being 3 nm in thickness, offering sufficient interface for stress and electron transfer in composites, and (3) cost-effectiveness (\$20/kg) [31–35]. Polyurethane (PU) is a multi-purpose polymer with the advantage of tailoring to meet demands; it can be molded in various forms including foams, thermoplastic elastomers, adhesives, and paintings. PU–nanofiller composites have been reported in plethora studies to improve mechanical performance [36, 37], and functional properties such as hydrophilicity [37], electrical conductivity [37], and piezo-resistivity's sensibility [38, 39].

Developing nanofiller-based sensors to detect numerous signals including—but not limited—mechanical strain, temperature change [40, 41], and pressure change [42] using nanofillers is an interest for both academia and industry. For example, Tang's group has investigated polyurethane/graphene oxide composite as multifunctional sensors to detect flame [40, 41] and organic vapor sensing [43]. Herein, we developed a flexible, highly sensitive and electrically conductive polyurethane (PU)/GnP composite film fabricated by a facile approach for wearable strain sensor. The flexible strain sensor has sandwich structure similar to the traditional strain sensor. The PU film was used as substrate with the advantage of excellent elasticity, ultra-lightweight, and non-toxicity. The PU/GnP thin film was used as strain gauge in a strain sensor system. The PU/GnP composite film demonstrates excellent electrical conductivity (1430 ± 50 S/cm) and high sensitivity (gauge factor up to 150), demonstrating high potential as a flexible strain sensor. It is as wearable strain sensor device achieving accurate monitoring for body motions such as pulse movement, cheek movement, and forearm muscle movement. Comparing with the previously demonstrated flexible strain sensor, our sensor realized accurate real-time monitoring for both low- and high-frequency body motions. Additionally, since fabrication of GnPs is simple and scalable compared to graphene oxide, our strain PU/GnP strain sensor has high potential in commercialization.

Figure 1 Schematic illustrates the fabrication procedures of graphene platelets film with digital images for the prepared film.



Experimental section

Materials

The graphite intercalation compound (GIC Asbury 1395) was kindly supplied by *Asbury Carbons*, NJ, USA. The elastomer that was used in this study is polyurethane (PU). A PU film – 0.04 mm in thickness—was purchased from local market which is widely used in medical treatment and leather industry. Acrylics pressure-sensitive adhesive was provided by *Shuhua Hengsheng* chemical company, Sichuan, China.

Fabrication of graphene platelets

GnPs were prepared by a published method [44]. In brief, the fabrication of GnPs is thermally expanding a commercial graphite intercalation compound in a crucible at 700 °C for 1 min. The thermal expansion converted the compounds into wormlike structure which is delaminated by ultrasonating for 2 h in acetone (under 20 °C); then, GnPs were produced after drying them in the oven overnight [30, 45].

Fabrication of GnP film

A glass mold was designed to load GnPs and then pressed them using two metal sheets with smooth surface to make GnPs into primary rectangular shape

with uniform thickness followed by further pressing the film using a hydraulic press for 1 min under 1 MPa pressure to form a thin GnP film. As shown in Fig. 1, this GnP film has good surface integrity, desirable flexibility, and uniform thickness.

Fabrications of strain sensor

Figure 2 illustrates the schematic of fabrication of strain sensor based on PU/GnP composite film. The sensor was assembled on an ultra-thin PU film. First, an acrylics pressure-sensitive adhesive was smeared over ultra-thin PU film (image a) and then placed a GnP film at the center area of the PU film (image b). An isotropic conductive adhesive (ICA) was painted at both ends of the GnP film connected to copper wires (image b). Another PU film with acrylics pressure-sensitive adhesive covered the top of the GnP film (image c). Finally, the composite film was pressed by the hydraulic press at 1 MPa for 1 min (image C). Eventually, a PU-GnP-PU sandwich is used as strain sensor (image d).

The average thicknesses of PU film and acrylics pressure-sensitive adhesive (APSA) are 0.04 ± 0.003 mm and ~ 0.01 mm, respectively. The thickness of GnP film depends on the weight of GnPs. The thickness of assembled composite film is equal to the sum of thicknesses of GnP film, PU film, and acrylics pressure-sensitive adhesive layer. Table 1

Figure 2 Schematic illustrations of the fabrication of strain sensor with digital photograph of strain sensor prepared.

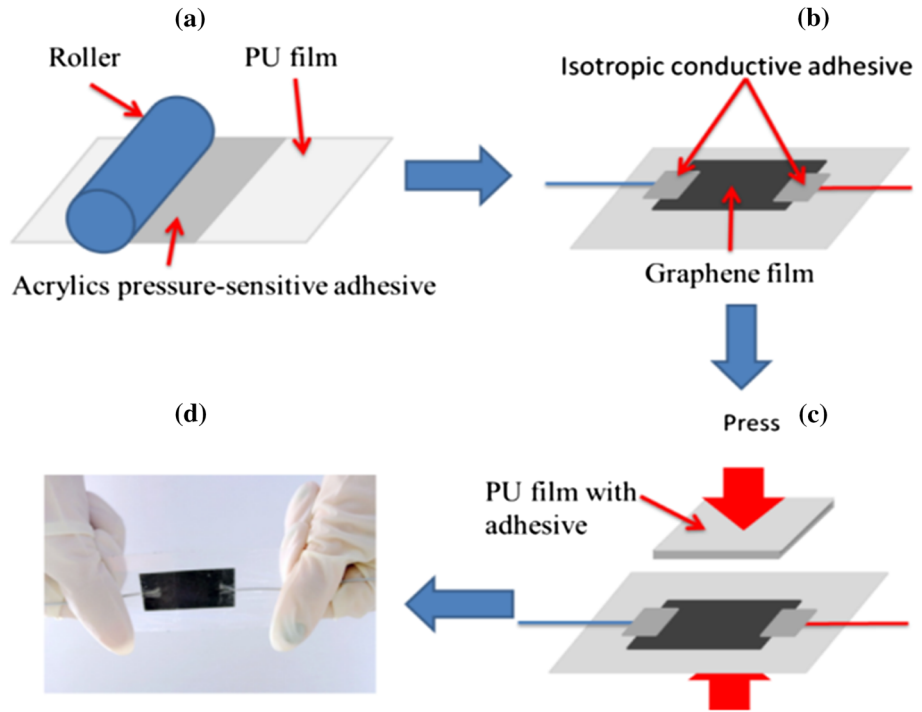


Table 1 The specification of GnP composite films

| Samples | Weight of GnPs (g) | Thickness of GnP film (mm) | Thickness of GnP composite film (mm) | Film size (mm) |
|---------|--------------------|----------------------------|--------------------------------------|----------------|
| 1 | 0 | 0 | 0.1 | 40 × 40 |
| 2 | 0.040 ± 0.005 | 0.02 ± 0.003 | 0.12 | 40 × 40 |
| 3 | 0.082 ± 0.005 | 0.05 ± 0.003 | 0.15 | 40 × 40 |
| 4 | 0.115 ± 0.005 | 0.07 ± 0.003 | 0.17 | 40 × 40 |
| 5 | 0.165 ± 0.005 | 0.10 ± 0.003 | 0.20 | 40 × 40 |

lists the specification of all the prepared GnP composite films.

Characterization

Scanning electron microscope (SEM) was conducted using a SEM (JEOL JSM-7800F) at 5 kV accelerating voltage. It was used to present images for the composite films’ cross section and surface. The high-magnification transmission electron microscope (TEM) images were taken from a JEOL microscope operated at 120 kV.

Mechanical properties were measured using Instron tensile testing machine at a cross-head speed of 2 mm/min at room temperature (25 °C). Young’s modulus and tensile strength of the samples were determined from the obtained stress–strain curves.

The sensitivity of the strain sensor is represented by the gauge factor (GF), that is, the ratio of the

changes in relative electrical resistance to the applied tensile strain. In order to investigate the sensitivity of the strain sensor, the GF of the composite films is calculated using the following equation:

$$GF = \frac{\Delta R/R_0}{\Delta L/L_0} = \frac{\Delta R/R_0}{\epsilon} \tag{1}$$

where R_0 is the initial resistance of the sensor, ΔR is the relative resistance change under deformation, L_0 is the initial length of the sensor, ΔL is the relative elongation of the film in the axial direction, and ϵ is the strain [46]. The strain was collected by Instron tensile machine at speed of 2 mm/min. FLUKE data acquisition unit was used to measure the electrical resistance of the strain sensor simultaneously while tensile testing was running; then, the GF was calculated according to the equation.

In the sensor applications section, the flexible strain sensor was glued on the skin surface and the FLUKE

data acquisition unit was used to measure the resistance of the flexible strain sensor. Similarly, the temperature and pressure responses were performed using the FLUKE data acquisition unit to record the resistance of flexible strain sensor under different pressure and temperature conditions. Program-controlled temperature furnace was used to control the temperature of the sensor from 20 to 150 °C at heating rate 1 °C/min. The hydraulic press was used to apply pressure on the sensor from 0 to 1000 kPa at room temperature (25 °C).

Results and discussion

Characterization of graphene platelets (GnPs)

Figure 3a illustrates high-resolution TEM micrographs of a typical GnP sheet. The ordered lines suggest the GnP sheet has intact crystalline structures. These crystalline structures reflect high electrical conductivity of GnP. This highly crystalline structure is in agreement with the X-ray photoelectron spectroscopy (XPS) analysis (Fig. 3b) which showed the C/O ratio is nearly 13.2 for GnPs. Thus, our GnPs would be a promising precursor for the fabrication of highly conductive sensors.

In Fig. 3c, GnPs lead to obvious absorptions at 1340 cm^{-1} , 1585 cm^{-1} , and 2690 cm^{-1} which correspond to D, G, and 2D bands, respectively. G band refers to sp^2 resonance on an ordered graphitic lattice, while D band is activated from the first-order scattering process of sp^2 carbons by the presence of in-plane substitutional hetero-atoms, vacancies, grain boundaries, or other defects, which might be sp^3 -

hybridized carbon structure associating with the quantity of impurity or oxidation degree. Since all samples were tested in the powder form, there is no point to discuss 2D band. The D- to G-band ratio of GnPs ($I_D/I_G = 0.07$) is much lower than those of other graphene derivatives and graphite [30, 47], revealing a far better structural integrity in case of our GnPs. These results also align with TEM and XPS analysis.

Morphology of PU/GnP composite film

Each of our GnP contains 1–4 layers of graphene sheets as reported previously [44, 45]. The GnP film was fabricated by pressing powder of GnPs forming a 2D overlap GnP film (illustrated in Fig. 2). Then, following the procedures mentioned in “Fabrications of strain sensor” section, a PU/GnP composite film was fabricated. A cross section of PU/GnP composite film of 0.17 mm in thickness was investigated using SEM imaging. Figure 4a shows the cross-sectional morphology of the composite film. The composite film shows a layered structure which consists of GnP film, acrylics pressure-sensitive adhesive (APSA), and PU layers. As shown in images b and c (Fig. 4), GnPs are tightly stacked and overlapped after pressing to form global conductive network. At high magnification, images d–f show the surface morphology of the GnP film; Fig. 4e demonstrates that the film has good surface integrity; Fig. 4d shows the connections and overlaps between adjacent platelets creating plenty of conductive paths. Figure 4f shows the micro-sized cracks and pores contained in the GnP film. Stress, strain, vibration, and other deformations cause the changes of conductive network resulting in dramatic resistance change mainly attributed to three mechanisms: (1) tunneling

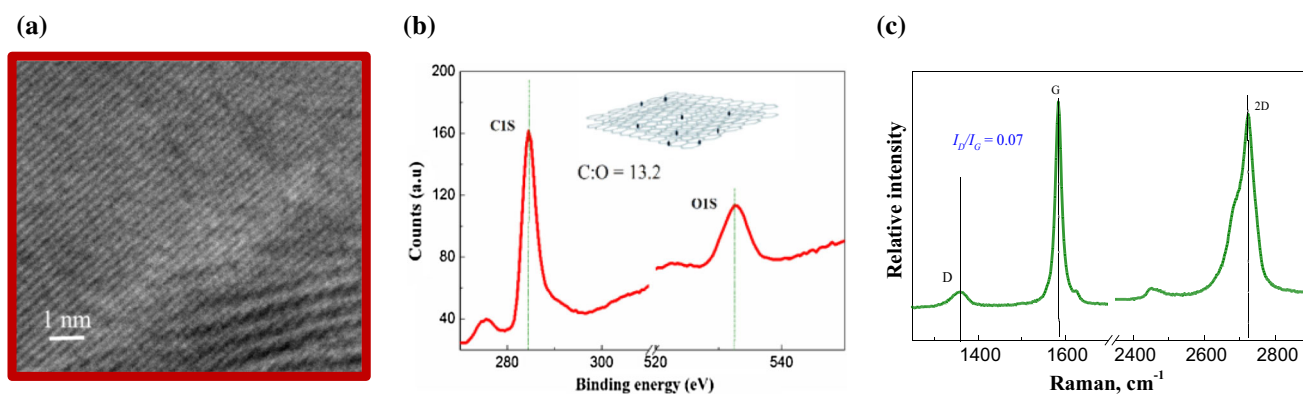


Figure 3 Morphology of graphene platelets: **a** high-resolution TEM image, **b** XPS analysis, and **c** Raman spectra.

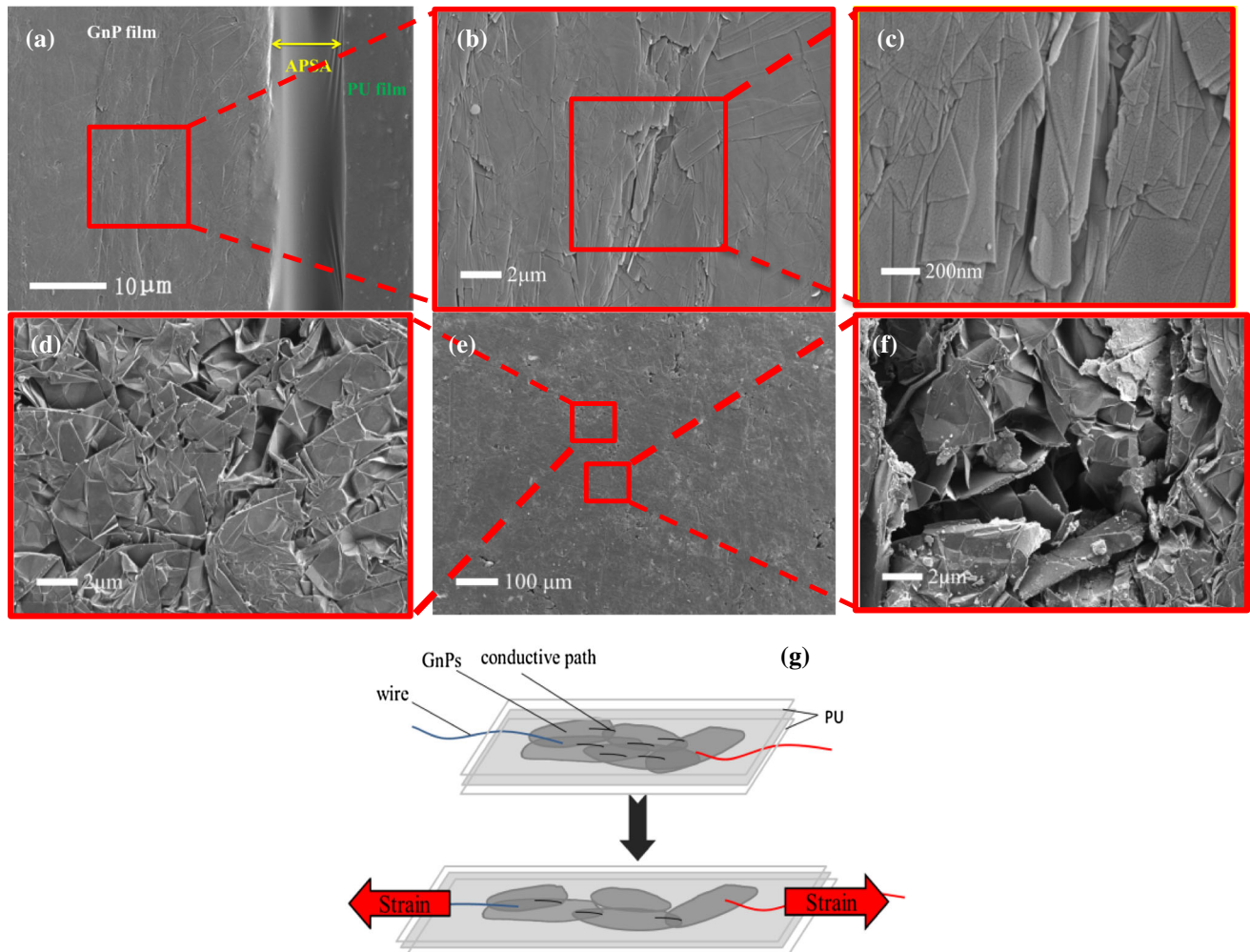


Figure 4 a–c Cross-sectional morphology of the composite film; d–f surface morphology of the GnP film; g schematic of sensor mechanism.

resistance change between adjacent platelets due to the expansion of micro-cracks, (2) influence of geometrical changes of GnP films, and (3) piezo-resistance of individual GnPs due to deformation upon loading [48]. The schematic in Fig. 4g demonstrates these mechanisms. In general, the resistance of a conductor is derived from the equation: $R = \rho \times L/A$, where ρ , L , and A are the specific resistivity, length, and cross-sectional area of the conductor, respectively. Thus, resistance change could be given by $\Delta R/R_0 = (1 + 2\nu)\varepsilon + \Delta\rho/\rho$, where the ν and ε are Poisson's ratio and strain, respectively. According to the equation, the resistance change is dependent on the strain and resistivity, and the resistivity of GnP stays the same after stretch [49]. Thus, the composite film could be used as a strain gauge of flexible strain sensor.

Mechanical performance

Young's moduli and tensile strengths are measured to investigate the mechanical performance of the composite films. Figure 5a shows the Young's moduli and tensile strengths of PU film and GnP composite films with different thicknesses. The thicknesses of the composite films are in range of 0.12–0.2 mm. Obviously, Young's moduli and tensile strengths are increasing with thickness. Since the PU films and acrylics pressure-sensitive adhesive (APSA) are identical for all GnP composite films while the weight of GnP is variable (Table 1), the improvement in mechanical properties is due to GnP's content; the larger thickness of GnP composite film is, the higher GnP's content is. The enhancement of strength and moduli of PU/GnP composite films are owing to the

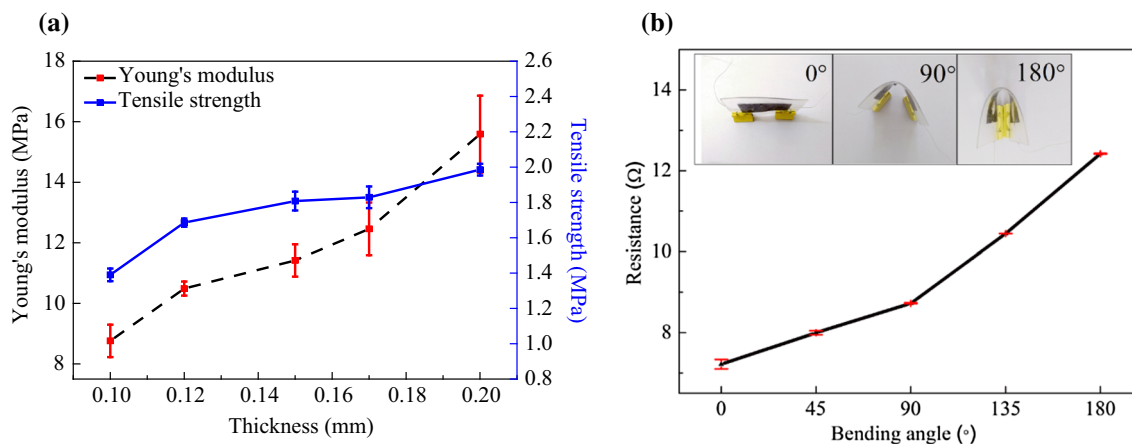


Figure 5 **a** Young's moduli and tensile strength of GnP composite films with different thicknesses; **b** the flexibility of a 0.17-mm-thick composite film.

increase in the rigid and high-strength phase (GnPs) in the composite. This is confirmed when comparing the results of samples 2–5 (thickness range 0.12–0.2 mm) which contain GnPs to sample 1 (thickness 0.1 mm) with no GnPs. It also indicates that the thicker films have stronger overlapped structure. Figure 5b shows the flexibility of the composite film of thickness 0.17 mm in which the composite film was bended into different angles, and the resistance increases with angles; however, the composite film still shows excellent electrical conductivity.

Sensitivity of strain sensor

Sensitivity is the key property for a strain sensor, which affects the performance of strain sensor directly [9]. Therefore, the gauge factor (GF) was employed to investigate the sensitivity of the strain sensor. Four GnP composite films with different thicknesses were examined to obtain their GF. Figure 6a is the schematic of GF testing in which the electrical resistance was measured when the tensile test was performing. Figure 6b is the fixture diagram of tensile machine. Figure 6c shows the relationship between electrical resistance changes and tensile strain of GnP composite films with different thicknesses. The result shows that the electrical resistance increases with strain due to the mechanisms discussed in “Morphology of PU/GnP composite film” section. Furthermore, the change in resistance (ΔR) decreases with the composite film thickness at same strain. By contrast, the black curve (0.12 mm) shows the highest (ΔR) among all other curves at same

strain range in Fig. 6c, while it is less linear with some fluctuations which could be caused by structural instability of thinner film, suggesting fewer GnP overlaps in the thickness direction and more micro-sized cracks. The other three curves show stable increase, and the green curve (0.20 mm) is most stable. In addition, the measurement range increases with thickness and the 0.17-mm- and 0.20-mm-thick films have wide measurement range of 0–25%. Figure 6d is the GF calculated by the result in Fig. 6c. In summary, the film with 0.12 mm thickness shows highest gauge factor but lowest linearity and smallest measurement range. The other films show better linearity and stable increased resistance. Therefore, based on both mechanical performance test and GF measurement, we chose the composite film with 0.17 mm thickness to fabricate the flexible strain sensor as the object of the following study.

Sensitivity of strain sensor

We then conducted cyclic tensile testing to study the stability and reproducibility of the strain sensor. The result exhibits good durability after 1000 cycles at 5% in Fig. 7a, the resistance changes of first 10 cycles and last 10 cycles are compared, and we found the waveform is roughly same, indicating the sensor has good stability and reproducibility thanks to the good elasticity of PU film and strong adhesion of the acrylics pressure-sensitive adhesive. Besides, a response time testing of the strain sensor was conducted and the result is shown in Fig. 7b; the strain sensor responds instantaneously to cyclic loading. We measured the response time

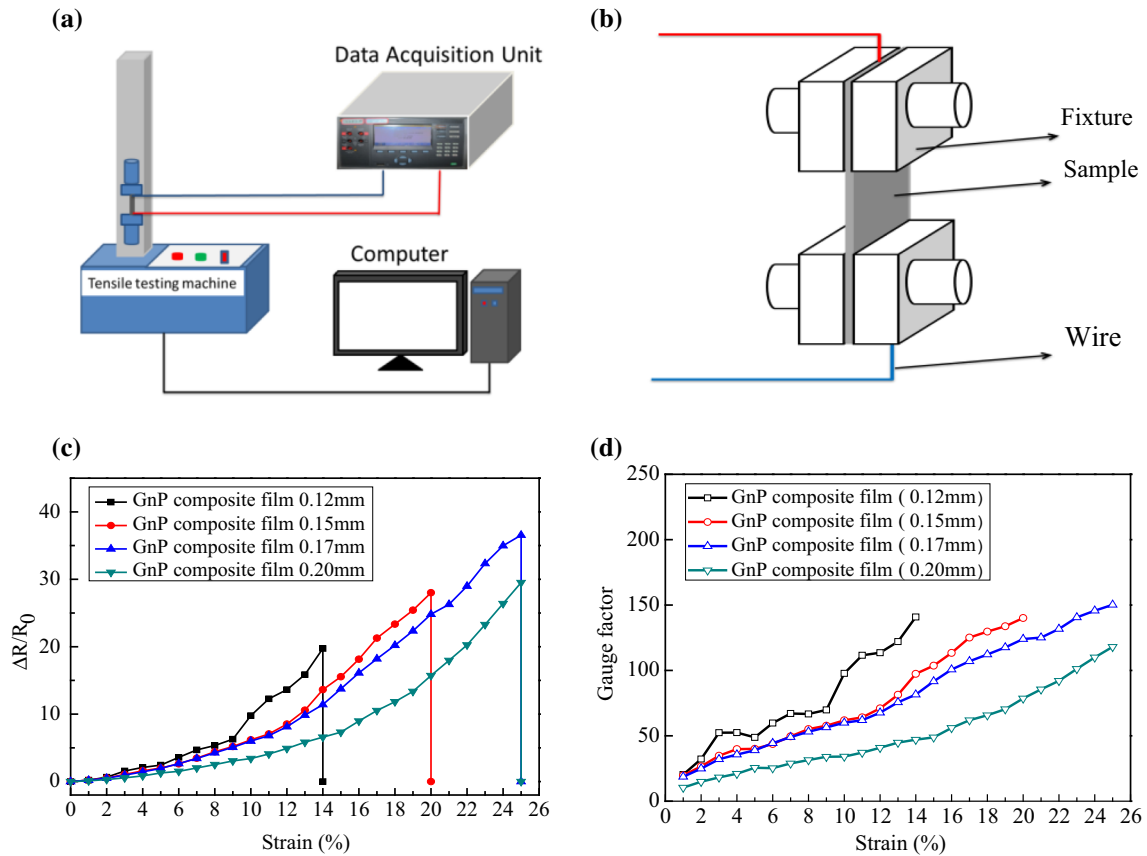


Figure 6 **a** Schematic of gauge factor testing; **b** the fixture schematic of tensile machine; **c** the curve of resistance changes and strain; **d** the curves of gauge factor and strain.

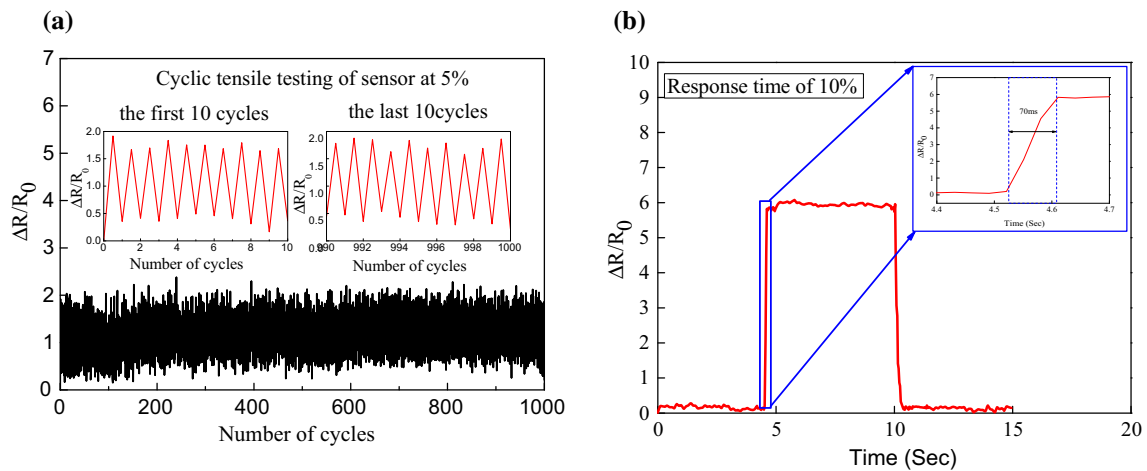


Figure 7 **a** Result of cyclic tensile testing of the sensor at 5%; **b** the response time testing of the sensor at 10%. 0.17 mm thickness strain sensor was used for all measurement.

when the strain sensor was applied 10% strain; it is 70 ms, indicating the flexible sensor has quick response ability. A good sensor requires not only

high sensitivity but also good stability and quick response ability. Obviously, our sensor meets these requirements.

Sensor application

As discussed previously, to be applied as wearable device for body motion measurement, the strain sensor needs to be flexible, highly sensitive, and light in weight [17, 50]. In this study, five typical body motions for wearable device including pulse, finger, cheek, forearm muscle movements, and human vocalization were investigated.

Figure 8 shows the flexible strain sensor used to monitor real-time pulse movement. Figure 8a is the schematic of pulse movement measurement, and the sensor was glued on the skin region where pulse movement is strongest. A photograph of the sensor was given in which the black part is GnP film and the transparent part is PU film. The pulse of an adult male's in the normal condition is around 12–13 beats per 10 s. The results recorded by our strain sensor accurately reflect the pulse movement of a healthy adult clearly (Fig. 8b). And the sensor achieves stable pulse movement monitoring. In order to

amplify the pulse signal and remove undesirable noise over faint pulse signal, we measured pulse movement again and used a 0.5–10 Hz band-pass filter on MATLAB at same time to filtrate the ambient noise. Figure 8c gives the comparison between the pulse waveforms before filter and after filter. The pulse waveform measured by our strain sensor highly agrees with the standard pulse waveform in Fig. 8d, even the percussion wave and the descending limb wave were observed [51, 52]. It is well known that pulse waveform signal is an important auxiliary parameter to examine whether the arterial blood vessels are normal. It can be used to predict hypertension, coronary heart disease, and other diseases, especially in hospital settings [53–55]. Therefore, our GnP composite films can be used as wearable device to monitor pulse movement to monitor a human body health.

Figure 9a shows the strain sensor recorded the behavioral changes when the fingers were repeatedly bended. The strain sensor was attached tightly on a

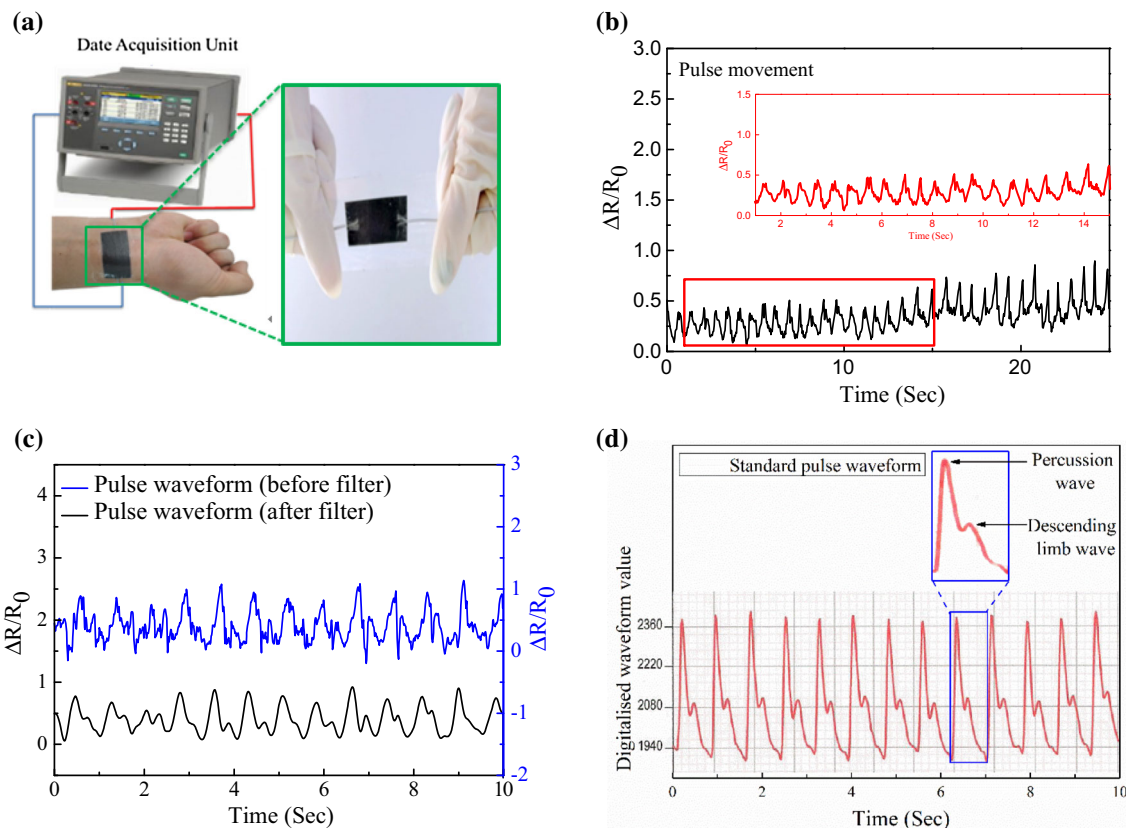


Figure 8 a Schematic of pulse movement measurement and photographs of the strain sensor; b the result of real-time monitoring for pulse movement; c pulse waveform contrast

between before filter and after filter; d the standard pulse waveform. 0.17 mm thickness strain sensor was used for all measurement.

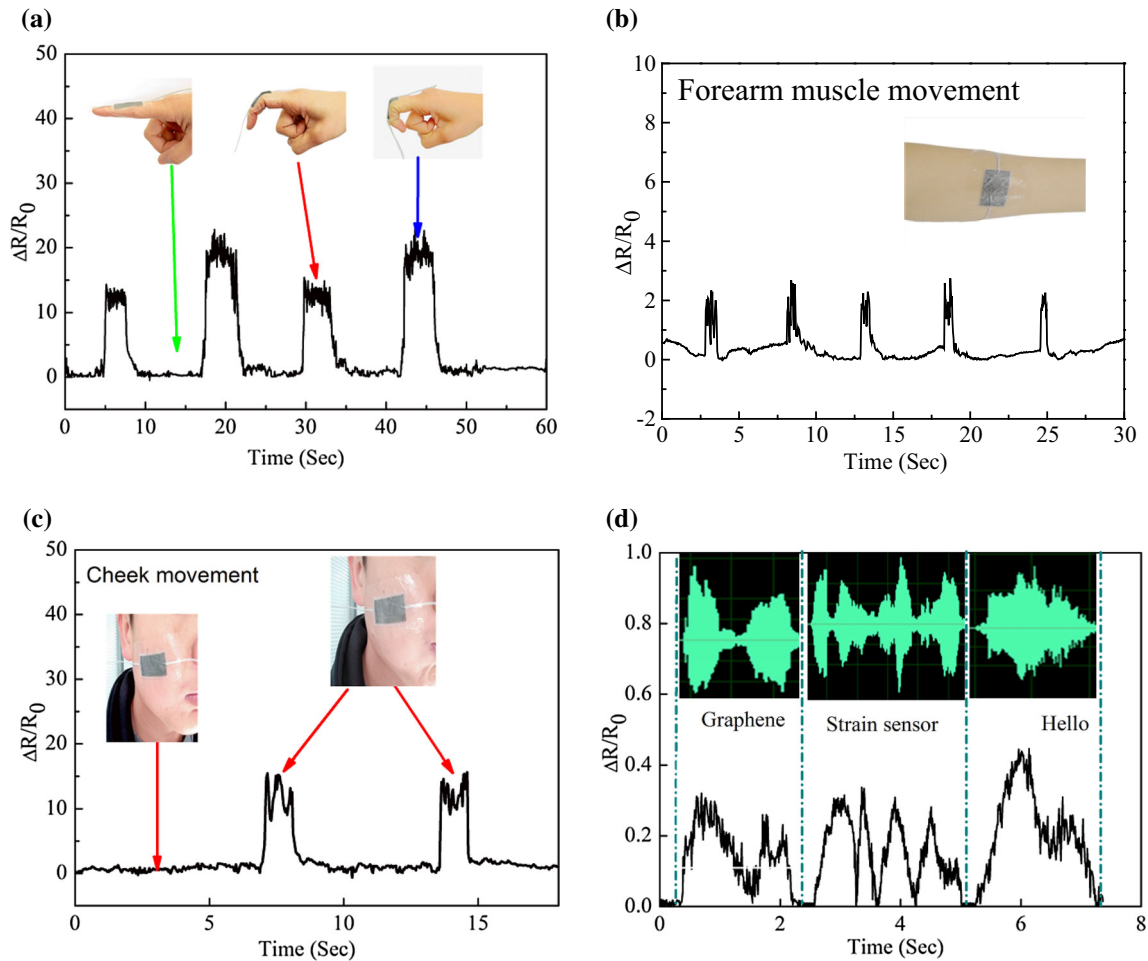


Figure 9 0.17 mm thickness strain sensor used to monitor **a** finger-bend movement, **b** forearm muscle movement, **c** cheek movement, and **d** voice vibration.

finger in straight state; the resistance of the sensor nearly remains constant with slight fluctuation. When the finger starts bending, the sensor would be stretched resulting in a sharp increase in resistance. Once the finger moves back to its original position, the resistance recovers instantly due to elasticity of the sensor. Meanwhile, the change of electrical resistance increases with the degree of finger bending motion.

In order to further check the wearable application of our sensor, another two subtle body motions were measured. Figure 9b, c shows the sensor used to monitor forearm muscle and cheek movement caused by muscle deformation. As shown in Fig. 9b, the sensor was glued on forearm, and when we clench, the brachioradialis would contract and cause a deformation perpendicular to the direction of the arm, forming a resistance change signal of the strain sensor. In Fig. 9b, the peak corresponds to the

clenching. The resistance of the sensor recovers with opening of the palm.

We proceeded to sense facial muscle movement, because facial expression recognition is vital for the development of human monitoring techniques. Figure 9c shows the strain sensor used to monitor cheek movement, which is a subtle body movement caused by risorius muscle deformation. There are two peaks corresponding to the bulge movement of cheek skin due to blowing. The left picture in Fig. 9c shows cheek in still state, and resistance of the strain sensor keeps stable. The right one is the cheek in movement state. When mouth is blowing, the resistance change reaches peak. This result indicates that our sensor has potential to monitor human facial emotion.

Human vocalization is based on muscle movement and vibration, and the sensor was attached onto the throat to identify various pronouncing of English

words. The result in Fig. 9d indicates that each signal curve of a word is apparently different to others, and similar to the wave shape of corresponding word, which provides evidence that our sensor can be used for voice recognition.

Temperature response and pressure response

Temperature has influence on electrical conductivity, and GF is temperature dependent [56, 57]. The resistance change caused by temperature is called temperature drift. The electrical resistance of the strain sensor was measured over a temperature range of 20–150 °C to study the temperature response.

Figure 10 shows the temperature–resistance curve. The resistance does not change significantly under 100 °C, while it increases sharply above 100 °C with more distinct error. According to the result, the strain sensor's appropriate operating temperature range is 20–100 °C, and temperature drift of the strain sensor in this range is too tiny to consider. On the other hand, resistance changes obviously when sensor temperature is beyond 100 °C. This is because the isotropic conductive adhesive (ICA) starts to lose its binding strength to the GnP film; the glass transition temperature of ICA is ~ 90 °C [58]. This would increase the electrical resistance at the interface between GnP film and ICA, and ICA with the copper wires which consequently increases the overall electrical resistance of the strain sensor. The viscous state of ICA explains the high standard deviation attained at temperature > 100 °C.

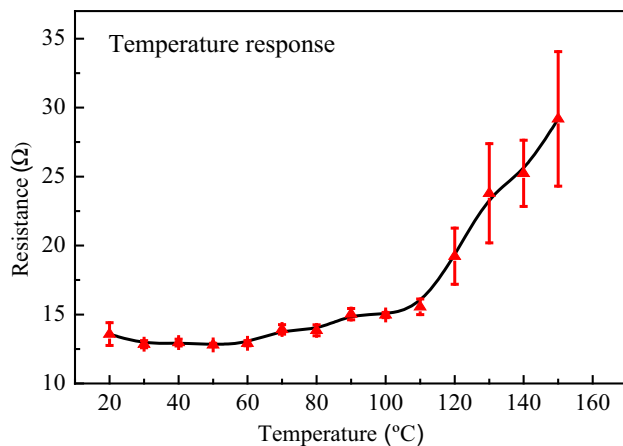


Figure 10 Temperature response of 0.17 mm thickness sensor.

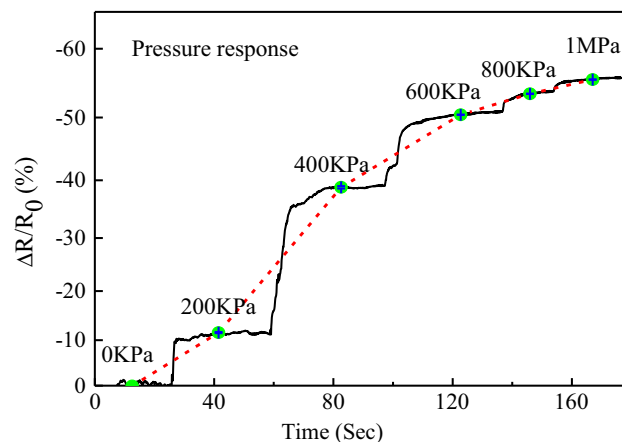


Figure 11 Resistance change of strain sensor of 0.17 mm thickness sensor at different pressures.

To evaluate the pressure response of the strain sensor, different levels of pressure were given to measure the electrical resistance of the strain sensor. Figure 11 shows the resistance of the strain sensor under pressure ranging from 0 to 1 MPa. The electrical resistance of the strain sensor decreases with the pressure, possibly due to the decrease in the interparticle distance and increase in GnP sheets connection and overlaps. The pressures on skin surface during body motions are generally not more than 10 kPa. For example, the pressure on skin surface of normal pulse movement is 5.33 kPa. The electrical resistance changes of the strain sensor under 10 kPa pressures are too tiny to observe. Thus, the resistance changes are mainly caused by strain in the sensor application as wearable device in this work. Besides, in Fig. 11, the sharpest decline is between 200 kPa and 600 kPa; therefore, the sensor could be used as a pressure sensor in the operating range of 200–600 kPa.

We have compared our PU/GnP flexible strain sensor with reported flexible strain sensors in terms of thickness, stretch ability, fabrication/difficulty, electrical conductivity, and wearable ability (Table 2). In contrast to the previously demonstrated flexible strain sensor, our strain sensor based on PU/GnP exhibits various advantages, including (1) high level of electrical conductivity (1430 S/cm), (2) high sensitivity (GF), (3) facile and cost-effective approach of fabrication, and (4) reliable bio-signal measurement. The GF of flexible strain sensor in this work is 255.45% higher than the strain sensor based on polydimethylsiloxane (PDMS)/graphene, 72.69%

Table 2 Comparison of flexible strain sensors fabricated by different materials

| Substrate/filler | Thickness (mm) | Fabrication/difficulty | Stretch ability (%) | Electrical conductivity (S/cm) | Gauge factor | Wearable ability | References |
|-------------------------|----------------|------------------------|---------------------|--------------------------------|--------------|------------------|------------|
| PU/MWCNTs | 1.6 | 3D print*** | 100 | 0.01 | 176 | + | [34] |
| PDMS/graphene | 0.12 | Spraying** | 20 | 0.42 | 42.2 | ++ | [59] |
| PU/PAN electrospun mats | 0.1–0.2 | Polymerization*** | 110 | 0.43 | 17.15 | + | [60] |
| PU core/graphene | 0.2 | Coating*** | 50 | 0.015 | 86.86 | + | [46] |
| Electrospun mats/RGO | 0.2 | Polymerization** | 250 | 0.002 | 79 | +++ | [61] |
| PU/GnP | 0.12–0.20 | LBL laminating* | 25 | 1430 ± 50 | 150 | +++++ | This work |

The number of “*” means the difficulty of corresponding fabrication which is measured by the fabrication time and process; one * is the lowest. The number of “+” means the number of the bio-signals measured in the paper

PDMS polydimethylsiloxane, PAN polyaniline, LBL layer by layer, RGO reduced graphene oxide

higher than PU core/graphene, and 89.87% higher than electrospun mats/RGO, respectively. High GF enables the strain sensor to detect the slight movement such as pulse movement accurately. In this work, we measured five bio-signals to study the wearable ability of our strain sensor. As shown, our strain sensor has greater potential to be used as wearable device because it has the ability to monitor both large and slight, low- and high-frequency movements.

Conclusion

In summary, we developed a highly sensitive and flexible strain sensor based on PU/GnP composite film fabricated by a facile approach. The flexible strain sensor was fabricated via layer-by-layer laminating method which is simple and cost-effective. The PU substrate gives the strain sensor good flexibility and stretch ability (up to 25%). The strain gauge made of GnP composite film achieves excellent electrical conductivity and high GF of 150, which is higher than the similar sensors reported. The cyclic tensile test shows our strain sensor has good stability and reproducibility after 1000 cyclic tensile test at 5% strain. For sensor applications, the flexible strain sensor successfully achieves accuracy monitoring for five body motions covering both large and slight, low- and high-frequency movements, and thus, it has good potential for wearable devices. In addition, the strain sensor has low-temperature drift in the operating temperature range of 0–100 °C, and it has the

ability of working in most condition of wearable device. According to the pressure response test of the strain sensor, the resistance changes are not influenced by pressure when the strain sensor was used as wearable device. Finally, we made a multifaceted comparison of different flexible strain sensors and summarized four advantages of our strain sensor including (1) high sensitivity (GF), (2) facile fabrication approach, and (3) various applications in wearable device.

Acknowledgements

QM and ZL thank Asbury and Huntsman (Melbourne) for providing the graphite intercalation compounds (1721 and 1395) and Jeffamine D 400, respectively. This work was financially supported by the Natural Science Foundation of Liaoning Province (20170520142). Dr. Tianqing Liu is supported by NHMRC Early Career Fellowship (1112258).

Compliance with ethical standards

Conflict of interest All authors declare that they have no conflict of interest.

References

- [1] Bae S-H, Lee Y, Sharma BK, Lee H-J, Kim J-H, Ahn J-H (2013) Graphene-based transparent strain sensor. Carbon 51:236–242. <https://doi.org/10.1016/j.carbon.2012.08.048>

- [2] Yamada T, Hayamizu Y, Yamamoto Y, Yomogida Y, Izadi-Najafabadi A, Futaba DN et al (2011) A stretchable carbon nanotube strain sensor for human-motion detection. *Nat Nanotechnol* 6(5):296–301. <https://doi.org/10.1038/nnano.2011.36>
- [3] Yu G, Hu J, Tan J, Gao Y, Lu Y, Xuan F (2018) A wearable pressure sensor based on ultra-violet/ozone microstructured carbon nanotube/polydimethylsiloxane arrays for electronic skins. *Nanotechnology* 29(11):115502. <https://doi.org/10.1088/1361-6528/aaa855>
- [4] Sakhaee-Pour A, Ahmadian MT, Vafai A (2008) Potential application of single-layered graphene sheet as strain sensor. *Solid State Commun* 147(7):336–340
- [5] Moriche R, Sánchez M, Jiménez-Suárez A, Prolongo SG, Ureña A (2016) Strain monitoring mechanisms of sensors based on the addition of graphene nanoplatelets into an epoxy matrix. *Compos Sci Technol* 123:65–70
- [6] Yang T, Jiang X, Zhong Y, Zhao X, Lin S, Li J et al (2017) A wearable and highly sensitive graphene strain sensor for precise home-based pulse wave monitoring. *ACS Sens* 2(7):967–974. <https://doi.org/10.1021/acssensors.7b00230>
- [7] Liu Y, Pharr M, Salvatore GA (2017) Lab-on-skin: a review of flexible and stretchable electronics for wearable health monitoring. *ACS Nano* 11(10):9614–9635. <https://doi.org/10.1021/acsnano.7b04898>
- [8] Pang Y, Tian H, Tao L, Li Y, Wang X, Deng N et al (2016) Flexible, highly sensitive, and wearable pressure and strain sensors with graphene porous network structure. *ACS Appl Mater Interfaces* 8(40):26458–26462. <https://doi.org/10.1021/acsami.6b08172>
- [9] Park JJ, Hyun WJ, Mun SC, Park YT, Park OO (2015) Highly stretchable and wearable graphene strain sensors with controllable sensitivity for human motion monitoring. *ACS Appl Mater Interfaces* 7(11):6317–6324. <https://doi.org/10.1021/acsami.5b00695>
- [10] Wang Y, Wang L, Yang T, Li X, Zang X, Zhu M et al (2014) Wearable and highly sensitive graphene strain sensors for human motion monitoring. *Adv Funct Mater* 24(29):4666–4670. <https://doi.org/10.1002/adfm.201400379>
- [11] Zha JW, Zhang B, Li RKY, Dang ZM (2016) High-performance strain sensors based on functionalized graphene nanoplates for damage monitoring. *Compos Sci Technol* 123:32–38
- [12] Moriche R, Jiménez-Suárez A, Sánchez M, Prolongo SG, Ureña A (2017) Graphene nanoplatelets coated glass fibre fabrics as strain sensors. *Compos Sci Technol* 146:59–64
- [13] Lee CJ, Jun S, Ju BK, Kim JW (2017) Pressure-sensitive strain sensor based on a single percolated Ag nanowire layer embedded in colorless polyimide. *Phys B Condens Matter* 514:8–12
- [14] Ho MD, Ling Y, Yap LW, Wang Y, Dong D, Zhao Y et al (2017) Percolating network of ultrathin gold nanowires and silver nanowires toward “invisible” wearable sensors for detecting emotional expression and apexcardiogram. *Adv Funct Mater* 27(25):1700845
- [15] Liu S, Lin Y, Wei Y, Chen S, Zhu J, Liu L (2017) A high performance self-healing strain sensor with synergetic networks of poly(ϵ -caprolactone) microspheres, graphene and silver nanowires. *Compos Sci Technol* 146:110–118
- [16] Zheng Y, Li Y, Dai K, Wang Y, Zheng G, Liu C et al (2018) A highly stretchable and stable strain sensor based on hybrid carbon nanofillers/polydimethylsiloxane conductive composites for large human motions monitoring. *Compos Sci Technol* 156:276–286
- [17] Zhan Z, Lin R, Tran VT, An J, Wei Y, Du H et al (2017) Paper/carbon nanotube-based wearable pressure sensor for physiological signal acquisition and soft robotic skin. *ACS Appl Mater Interfaces* 9(43):37921–37928. <https://doi.org/10.1021/acsami.7b10820>
- [18] Huang W, Dai K, Zhai Y, Liu H, Zhan P, Gao J et al (2017) Flexible and lightweight pressure sensor based on carbon nanotube/thermoplastic polyurethane-aligned conductive foam with superior compressibility and stability. *ACS Appl Mater Interfaces* 9(48):42266–42277. <https://doi.org/10.1021/acsami.7b16975>
- [19] Araby S, Meng Q, Zhang L, Kang H, Majewski P, Tang Y et al (2014) Electrically and thermally conductive elastomer/graphene nanocomposites by solution mixing. *Polymer* 55(1):201–210. <https://doi.org/10.1016/j.polymer.2013.11.032>
- [20] Yan Y, Potts M, Jiang Z, Sencadas V (2018) Synthesis of highly-stretchable graphene–poly(glycerol sebacate) elastomeric nanocomposites piezoresistive sensors for human motion detection applications. *Compos Sci Technol* 162:14–22
- [21] Hao B, Mu L, Ma Q, Yang S, Ma PC (2018) Stretchable and compressible strain sensor based on carbon nanotube foam/polymer nanocomposites with three-dimensional networks. *Compos Sci Technol* 163:162–170
- [22] Nie B, Li X, Shao J, Li X, Tian H, Wang D et al (2017) Flexible and transparent strain sensors with embedded multiwalled carbon nanotubes meshes. *ACS Appl Mater Interfaces* 9(46):40681–40689. <https://doi.org/10.1021/acsami.7b12987>
- [23] Zhang S, Zhang H, Yao G, Liao F, Gao M, Huang Z et al (2015) Highly stretchable, sensitive, and flexible strain sensors based on silver nanoparticles/carbon nanotubes composites. *J Alloys Compd* 652:48–54. <https://doi.org/10.1016/j.jallcom.2015.08.187>

- [24] Christ JF, Aliheidari N, Ameli A, Pötschke P (2017) 3D printed highly elastic strain sensors of multiwalled carbon nanotube/thermoplastic polyurethane nanocomposites. *Mater Des* 131:394–401. <https://doi.org/10.1016/j.matdes.2017.06.011>
- [25] Geim AK (2009) Graphene: status and prospects. *Science* 324(5934):1530–1534. <https://doi.org/10.1126/science.1158877>
- [26] Materials N (2007) The rise of graphene. *Nat Mater* 6(3):183–191
- [27] Banhart F, Kotakoski J, Krasheninnikov AV (2011) Structural defects in graphene. *ACS Nano* 5(1):26–41. <https://doi.org/10.1021/nn102598m>
- [28] Potts JR, Dreyer DR, Bielawski CW, Ruoff RS (2011) Graphene-based polymer nanocomposites. *Polymer* 52(1):5–25. <https://doi.org/10.1016/j.polymer.2010.11.042>
- [29] Zhu Y, Murali S, Cai W, Li X, Suk JW, Potts JR et al (2010) Graphene and graphene oxide: synthesis. *Prog Appl* 22(35):3906–3924. <https://doi.org/10.1002/adma.201001068>
- [30] Zaman I, Kuan HC, Meng Q, Michelmore A, Kawashima N, Pitt T et al (2012) A facile approach to chemically modified graphene and its polymer nanocomposites. *Adv Funct Mater* 22(13):2735–2743
- [31] Ma J, Meng Q, Zaman I, Zhu S, Michelmore A, Kawashima N et al (2014) Development of polymer composites using modified, high-structural integrity graphene platelets. *Compos Sci Technol* 91(2):82–90
- [32] Shi G, Araby S, Gibson CT, Meng Q, Zhu S, Ma J (2018) Graphene platelets and their polymer composites: fabrication, structure, properties, and applications. *Adv Funct Mater* 28:1706705
- [33] Meng Q, Wu H, Zhao Z, Araby S, Lu S, Ma J (2017) Free-standing, flexible, electrically conductive epoxy/graphene composite films. *Compos A Appl Sci Manuf* 92:42–50
- [34] Araby S, Saber N, Ma X, Kawashima N, Kang H, Shen H et al (2015) Implication of multi-walled carbon nanotubes on polymer/graphene composites. *Mater Des* (1980–2015) 65:690–699. <https://doi.org/10.1016/j.matdes.2014.09.069>
- [35] Araby S, Zhang L, Kuan H-C, Dai J-B, Majewski P, Ma J (2013) A novel approach to electrically and thermally conductive elastomers using graphene. *Polymer* 54(14):3663–3670. <https://doi.org/10.1016/j.polymer.2013.05.014>
- [36] Cao C-F, Zhang G-D, Zhao L, Gong L-X, Gao J-F, Jiang J-X et al (2019) Design of mechanically stable, electrically conductive and highly hydrophobic three-dimensional graphene nanoribbon composites by modulating the interconnected network on polymer foam skeleton. *Compos Sci Technol* 171:162–170. <https://doi.org/10.1016/j.compscitech.2018.12.014>
- [37] Qiang F, Hu L-L, Gong L-X, Zhao L, Li S-N, Tang L-C (2018) Facile synthesis of super-hydrophobic, electrically conductive and mechanically flexible functionalized graphene nanoribbon/polyurethane sponge for efficient oil/water separation at static and dynamic states. *Chem Eng J* 334:2154–2166. <https://doi.org/10.1016/j.cej.2017.11.054>
- [38] Tan Y-J, Li J, Chen Y-F, Tang X-H, Cai J-H, Liu J-H et al (2019) Gentle crosslinking to enhance interfacial interaction in thermoplastic polyurethane/poly(ethylene-co-1-octene)/multi-walled carbon nanotube composites for conductive improvement and piezoresistive stability. *Polym Test* 75:142–150. <https://doi.org/10.1016/j.polymertesting.2019.02.004>
- [39] Cai J-H, Chen Y-F, Li J, Tan Y-J, Liu J-H, Tang X-H et al (2019) Asymmetric deformation in poly(ethylene-co-1-octene)/multi-walled carbon nanotube composites with glass micro-beads for highly piezoresistive sensitivity. *Chem Eng J* 370:176–184. <https://doi.org/10.1016/j.cej.2019.03.223>
- [40] Xu H, Li Y, Huang N-J, Yu Z-R, Wang P-H, Zhang Z-H et al (2019) Temperature-triggered sensitive resistance transition of graphene oxide wide-ribbons wrapped sponge for fire ultrafast detecting and early warning. *J Hazard Mater* 363:286–294. <https://doi.org/10.1016/j.jhazmat.2018.09.082>
- [41] Wu Q, Gong L-X, Li Y, Cao C-F, Tang L-C, Wu L et al (2018) Efficient flame detection and early warning sensors on combustible materials using hierarchical graphene oxide/silicone coatings. *ACS Nano* 12(1):416–424. <https://doi.org/10.1021/acsnano.7b06590>
- [42] Wang M, Zhang K, Dai X-X, Li Y, Guo J, Liu H et al (2017) Enhanced electrical conductivity and piezoresistive sensing in multi-wall carbon nanotubes/polydimethylsiloxane nanocomposites via the construction of a self-segregated structure. *Nanoscale* 9(31):11017–11026. <https://doi.org/10.1039/C7NR02322G>
- [43] Qiang F, Dai S-W, Zhao L, Gong L-X, Zhang G-D, Jiang J-X et al (2019) An insulating second filler tuning porous conductive composites for highly sensitive and fast responsive organic vapor sensor. *Sens Actuators B Chem* 285:254–263. <https://doi.org/10.1016/j.snb.2019.01.043>
- [44] Zaman I, Kuan HC, Dai J, Kawashima N, Michelmore A, Sovi A et al (2012) From carbon nanotubes and silicate layers to graphene platelets for polymer nanocomposites. *Nanoscale* 4(15):4578–4586. <https://doi.org/10.1039/c2nr30837a>
- [45] Qingshi M, Jian J, Ruoyu W, Hsu-Chiang K, Jun M, Nobuyuki K et al (2014) Processable 3-nm thick graphene platelets of high electrical conductivity and their epoxy composites. *Nanotechnology* 25(12):125707
- [46] Li X, Hua T, Xu B (2017) Electromechanical properties of a yarn strain sensor with graphene-sheath/polyurethane-core.

- Carbon 118:686–698. <https://doi.org/10.1016/j.carbon.2017.04.002>
- [47] Ma J, Meng Q, Michelmore A, Kawashima N, Izzuddin Z, Bengtsson C et al (2013) Covalently bonded interfaces for polymer/graphene composites. *J Mater Chem A* 1(13):4255–4264
- [48] Shi G, Zhao Z, Pai J-H, Lee I, Zhang L, Stevenson C et al (2016) Highly sensitive, wearable, durable strain sensors and stretchable conductors using graphene/silicon rubber composites. *Adv Funct Mater* 26(42):7614–7625. <https://doi.org/10.1002/adfm.201602619>
- [49] Nakamura A, Hamanishi T, Kawakami S, Takeda M (2017) A piezo-resistive graphene strain sensor with a hollow cylindrical geometry. *Mater Sci Eng B* 219:20–27. <https://doi.org/10.1016/j.mseb.2017.02.012>
- [50] Ryu S, Lee P, Chou JB, Xu R, Zhao R, Hart AJ et al (2015) Extremely elastic wearable carbon nanotube fiber strain sensor for monitoring of human motion. *ACS Nano* 9(6):5929–5936. <https://doi.org/10.1021/acs.nano.5b00599>
- [51] Wilkinson IB, Hall IR, MacCallum H, Mackenzie IS, McEniery CM, van der Arend BJ et al (2002) Pulse-wave analysis: clinical evaluation of a noninvasive, widely applicable method for assessing endothelial function. *Arterioscler Thromb Vasc Biol* 22(1):147–152
- [52] Bortel LM, Van SL, Pierre B, Phil C, Cruickshank JK, Tine DB et al (2012) Expert consensus document on the measurement of aortic stiffness in daily practice using carotid-femoral pulse wave velocity. *J Hypertens* 30(3):445–448
- [53] Xuewen W, Yang G, Zuoping X, Zheng C, Ting Z (2014) Silk-molded flexible, ultrasensitive, and highly stable electronic skin for monitoring human physiological signals. *Adv Mater* 26(9):1336–1342
- [54] O'Rourke MF, Pauca A, Jiang XJ (2001) Pulse wave analysis. *Br J Clin Pharmacol* 51(6):507–522
- [55] Koydemir HC, Ozcan A (2018) Wearable and implantable sensors for biomedical applications. *Annu Rev Anal Chem (Palo Alto Calif)* 11(1):127–146. <https://doi.org/10.1146/annurev-anchem-061417-125956>
- [56] Sayed S, Gamil M, Fath El-Bab AMR, Abd Elmoneim AAEM (2015) Laser reduced graphene on flexible substrate for strain sensing applications: temperature effect on gauge factor. *Key Eng Mater* 644:115–119
- [57] Bower DI (1972) Temperature dependence of gauge factor and magnetoresistance of some platinum-tungsten strain gauges. *J Phys E Sci Instrum* 5(9):846–848. <https://doi.org/10.1088/0022-3735/5/9/002>
- [58] Yim MJ, Paik KW (2006) Review of electrically conductive adhesive technologies for electronic packaging. *Electron Mater Lett* 2(3):183–194
- [59] Chun S, Choi Y, Park W (2017) All-graphene strain sensor on soft substrate. *Carbon* 116:753–759. <https://doi.org/10.1016/j.carbon.2017.02.058>
- [60] Tian M, Wang Y, Qu L, Zhu S, Han G, Zhang X et al (2016) Electromechanical deformation sensors based on polyurethane/polyaniline electrospinning nanofibrous mats. *Synth Met* 219:11–19. <https://doi.org/10.1016/j.synthmet.2016.05.005>
- [61] Wang Y, Hao J, Huang Z, Zheng G, Dai K, Liu C et al (2018) Flexible electrically resistive-type strain sensors based on reduced graphene oxide-decorated electrospun polymer fibrous mats for human motion monitoring. *Carbon* 126:360–371. <https://doi.org/10.1016/j.carbon.2017.10.034>

Publisher's Note Springer Nature remains neutral with regard to jurisdictional claims in published maps and institutional affiliations.